World Journal of Engineering Research
ISSN: 2959-9873
DOI: https://doi.org/10.61784/wjer3022

REPRODUCE LONG-TAIL CURRENT HYSTERESIS IN PEROVSKITE SOLAR CELLS BASED ON AN IONIC CAPACITOR MODELLED BY A VOLTAGE-RELATED INITIAL CURRENT TIMES THE LINEAR COMBINATION OF THREE EXPONENTIAL DECAY TERMS

Biao Peng, RongXin Wu, YueWen Chen, MuYun Li, YingFeng Li*
State Key Laboratory of Alternate Electrical Power System with Renewable Energy Sources, School of Renewable Energy, North China Electric Power University, Beijing 102206, China.
Corresponding Author: YingFeng Li, Email: liyingfeng@ncepu.edu.cn

Abstract: It has been reported that the current-voltage (J-V) hysteresis loop of perovskite solar cells (PSCs) could be reproduced by incorporating extra resistances or capacitors in the equivalent circuits of PSCs. However, the exponential decay long-tail current in the hysteresis phenomenon, lasting about 2-5 seconds, remains inadequately modeled, yet it is crucial for maximum power point tracking in PSCs. We propose an ionic capacitor model to describe the impact of ion migration on the current of PSCs, which is composed of a voltage-related initial current multiplies by the linear combination of three exponential decay terms over time. The initial current term is formulated as the product of the voltage step size and a voltage-related conductance. The three exponential terms, each associated with a specific time constants τ, correspond to the migration of electron, iodine ions, and other ions with lower mobilities, respectively. Based on this model, an equivalent circuit for PSCs is constructed, and corresponding parameters were numerical fitted based on available *J-V* data and current-time response curves. Numerical simulations demonstrate that the proposed model accurately reproduces both the *J-V* hysteresis loop and the exponential decay long-tail current. This work lays the foundation for the development of MPPT tracking algorithms tailored for PSCs.
Keywords: Perovskite solar cells; Hysteresis; Long-tail current; Ionic capacitor

1 INTRODUTION

Recently, perovskite solar cells (PSCs) have garnered significant attention in the research community[1-4]. These cells can be manufactured using solution-based methods, offering low production and material costs, which gives them advantages over traditional crystalline silicon solar cells. To date, the photoelectric conversion efficiencies of PSCs have reached 27.0%[5]. With the industrialization and practical applications of PSCs in power generation, maximum power point tracking (MPPT) has become indispensable. Common MPPT algorithms include the perturb and observe (P&O) method and the incremental conductance method (INC)[6-7]. Both algorithms require continuous adjustments to the battery's output voltage to locate the maximum power point, and their determination of the maximum power point's location is based on the battery's *J-V* characteristic curve[8].

Actually, adjusting the output voltage during the MPPT process in solar cell is equivalent to altering the electric field across the cell. In addition to conventional electrons, various ions in perovskite solar cells (PSCs) can also migrate in response to an external electric field. These migrated ions under the electric field will accumulate or dissipate at the electron transport layer (ETL)/perovskite interface and the hole transport layer (HTL)/perovskite interface. These ion accumulation and dissipation processes in response to the changing electric field are equivalent to introducing a series capacitor, characterized by a long charge-discharge time constant, within the PSC. This complex ion migration behavior is just the underlying mechanism behind the well-known hysteresis effect[10-11]. The hysteresis effect of PSCs shows two key characteristics. The first one is the non-overlapping current-voltage (*J-V*) curves during the forward and reverse scan of the PSCs, usually called the hysteresis loop, as illustrated in Figure 1(a). The other characteristic is the time-dependent decay of the dynamic non-steady-state photocurrent during stepwise voltage scanning, with a response time ranging from 2-5 seconds[9], which is named “long-tail current” in this work, as shown in Figure 1(b) and 1(c). This hysteresis effect renders conventional MPPT techniques unsuitable for PSCs[8].

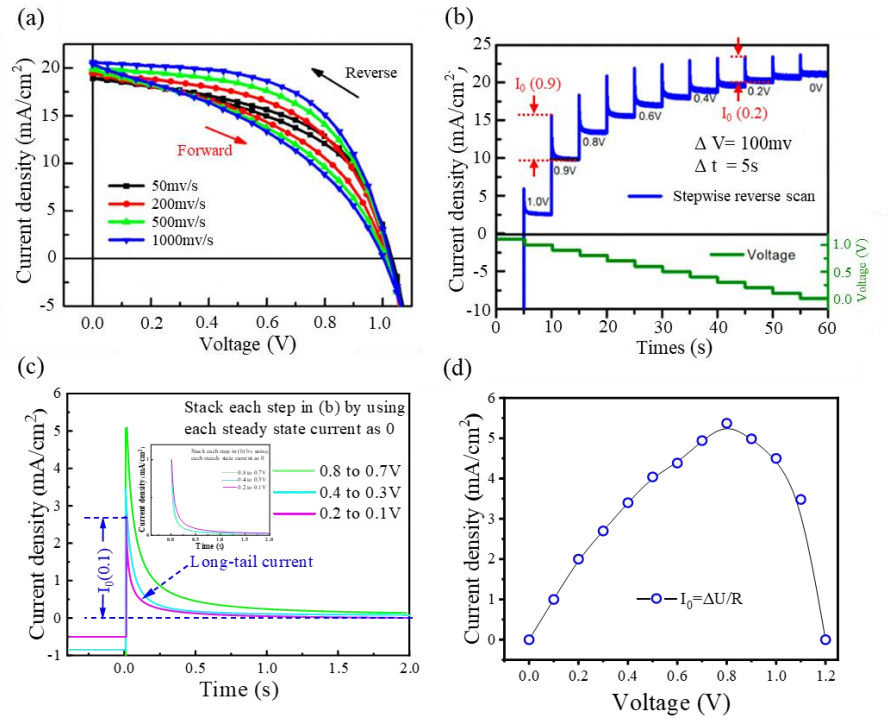

Figure 1 (a) Hysteresis Loops of PSC under Different Scan Rates; (b) Time-dependent Photocurrent Response under Stepwise Reverse Scan with 100 mV Step Size and 5 s Step Time; (c) Decay of Dynamic Non-Steady-State Photocurrent with Time during the Stepwise Reverse Scan, the Inset Figure is the Normalized Exponential Decay Current Curves; (d) The Initial Current Extracted from (b) Changes with Voltage. Reprinted (adapted) with Permission from ref 18. Copyright © 2015, American Chemical Society

A critical step in constructing new MPPT algorithms for PSCs is to develop a model that can quantitatively describe the impact of ion migration on the hysteresis effect. In previous reports, the ion migration behaviors were modeled using a conventional electronic capacitor in parallel with an appropriate resistance[12-13]. Seki et al. have integrated such a parallel resistor-capacitor (RC) module (fixed resistor in parallel with fixed capacitor) in series into an equivalent circuit model of PSCs[14], and reproduced the hysteresis loop in both forward and reverse *J-V* sweep curves. However, such a simplified model effectively abstracts various carriers, including electrons and ions, in PSCs into a kind of "pseudo carrier" with lower carrier mobility. As a consequence, the long-tail current in PSCs, characterized by multiple segments corresponding to the migration of different ions, cannot be accurately reproduced[15].

Aware of this defect, J. B et al. have studied the long-tail current response of PSCs in response to a small voltage perturbation of 10 mV over a steady-state of 1 V[16]. They have divided the long-tail current into three distinct segments and modeled each segment using different RC/RL circuits. Based on impedance spectroscopy measurements, they fitted the parameters in the RC/RL circuits. Such constructed model reproduced the long-tail current curve under a given voltage very well. However, this model is also difficult to directly apply in MPPT algorithm design. On one hand, the parameters extraction rely on additional impedance spectroscopy measurements, on the other hand, it lacks to establish an analytical relationship between the model parameters and the voltage.

2 IONIC CAPACITOR MODEL

For crystalline silicon solar cells, changing the voltage will disrupt the equilibrium of the built-in field, driving charge carriers (electrons and holes) to flow through the external circuit, as illustrated in Figure 2a, thereby generating current. In contrast, PSCs exhibit a different mechanism. Under the voltage changing not only electrons but also various ions migrate toward the respective transport layers. Due to the selective permeability of the ETL/HTL, these ions cannot fully penetrate the interfaces and instead accumulate at the surface, as illustrated in Figure 2b**.** These accumulated ions can act as an equivalent resistance which affects the electron transport. However, since the migration processes take time, it can be resembled as the charging and discharging behavior of a capacitor. Therefore, we use an ionic capacitor to describe the impacts of ions migration behavior on the electron transport.

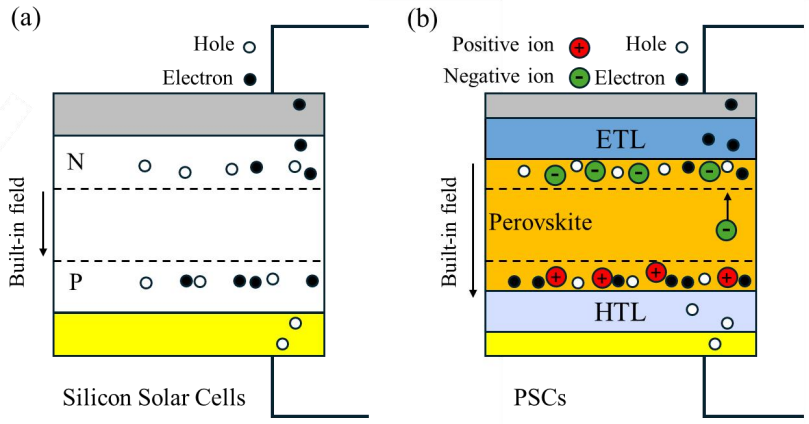

Figure 2 The Electric Field and Carrier Dynamics in (a) Crystalline Silicon Solar Cells and (b) PSCs

To accurately reflect the long-tail current effect, referring to the model proposed by J.B. et al. [16], we have modified the conventional electronic capacitor into a linear combination of three different capacitors. The modeling process is as follows. According to the Kirchhoff laws, the charging or discharging current of a capacitor can be expressed by equation 1,

$$I_c(t) = (U - \frac{Q(t)}{C})/R \tag{1}$$

where U is the apply voltage, $Q(t)$ is the charge on the conductor at time t, C denotes the capacitance, R is the external resistance. By substituting into equation (1) and solving the resulting first-order differential equation, we obtained

$$Q(t) = CU - \xi Ce^{-\frac{t}{RC}} \tag{2}$$

The integration constant can be determined by setting $t=0$, After substituting into equation (2), the charging or discharging current of the capacitor can be derived by differentiating $Q(t)$ with respect to t,

$$I_c(t) = \frac{dQ(t)}{dt} = \frac{Q(0)/C-U}{R}e^{-\frac{t}{RC}} = \frac{U_0-U}{R}e^{-\frac{t}{RC}} \tag{3}$$

where represents the voltage on the capacitor before adjustment. can be represented as ΔU, which represents the voltage adjustment step size. The reciprocal of the external resistance R can be expressed as the conductivity σ. Meanwhile, the charging or discharging time constant of the capacitor with external resistance R, given by RC, can be denoted by τ. The time response equation of a given capacitor can be written as

$$I_c(t) = \Delta U\sigma e^{-t/\tau} = I_0 e^{-t/\tau} \tag{4}$$

The first term, $I_0=\Delta U\sigma$, describes the initial current value on the capacitor after a voltage adjustment; and the second term, $e^{-t/\tau}$, corresponds to decay speed of the capacitor current over time.

As discussed above, the capacitor current in PSCs is not solely due to electron migration but is also influenced by the migration of various ions, including fast-moving species such as I^- and slower-moving ions like MA^+. Therefore, we try to interpret the capacitor current in PSCs as the joint contribution of three distinct carriers,

$$I_c(t) = I_0^1 e^{-t/\tau_1} + I_0^2 e^{-t/\tau_2} + I_0^3 e^{-t/\tau_3} \tag{5}$$

In this equation, the three terms represent the contributions of electron migration, fast-moving ion migration, and slow-moving ion migration, respectively. I_0^1, I_0^2, and denote the initial currents contributed by the three types of charge carriers, while τ_1, τ_2, and represent the time constants of the three sub-capacitors. However, in practical measurements, directly obtaining the initial currents associated with individual charge carriers is unfeasible. Instead, an overall initial current of the capacitor in PSCs can be conveniently derived from time-dependent photocurrent measurements. Considering this fact, we reformulate equation 5 by replacing the individual initial currents with an overall initial current, I_0, while representing the contributions of different carriers through weighting factors c_1, c_2, and c_3,

$$I_c(t) = I_0(c_1 e^{-t/\tau_1} + c_2 e^{-t/\tau_2} + c_3 e^{-t/\tau_3}) \tag{6}$$

The values of I_0 under various voltages were extracted from Figure 1(b) and plotted in Figure 1(d). It can be observed that I_0 increases first and then decreases with the increase of the voltage. This is because $I_0=\Delta U/R$, while R, which characterizes the influence of ion migrations on charge trapping and defect-induced recombination[17], should be voltage-dependent. As the reciprocal of R, the conductivity should be also voltage-dependent. However, due to the complexity of the origins of R, it is challenging to establish a physically meaningful equation to describe the relationship between and U. Here, we adopt a mathematically feasible approach, namely a polynomial function, to express this relationship,

$$I_0 = \Delta U\sigma(U) = \Delta U(aU^4 + bU^3 + cU^2 + dU + e) \tag{7}$$

3 NUMERICAL FITTING AND MODEL CONSTRUCTION

To determine the parameters in equation 7, we extracted data for I_0 at various voltages (25℃, 1000W/m^2) from the

measured data of Bo Chen et al.[18], as shown in Figure 1(d) and performed regression fitting to determine the parameters in equation 7. The obtained expression of I_0 is shown in equation 7, with *R-square =0.964*.

$$I_0 = 0.1 * (-320.9U^4 + 242.9U^3 + 18.25U^2 + 10720U + 2.428) \quad (8)$$

The three exponential current decay terms in equation 6 represent the contributions of electron migration, fast-moving ion migration, and slow-moving ion migration, respectively. The first term is primarily responsible for the rapid decay in the initial stage of the long-tail response in PSCs[16, 19-20] within small than one second. It has been widely confirmed that iodide ions are the majority of migrating ions in PSCs, and the local electric field established by their migration results in a current decay over a longer time scale[17]. The second term takes account for the influence of the local electric field formed by iodide migration on the charge capture behaviors in PSCs. There are also some other slow-moving ions, like MA^+ or bound iodide ions, in PSCs[20]. To capture the effects of these slow-moving ions, we introduced the third term.

Then, regarding the long-tail exponential current decay term, the normalized curves in Figure 1c show that the differences in decay curves under varying voltages are not particularly significant and do not critically impact the manifestation of the hysteresis effect. For the convenience of fitting, we selected the representative current response curve corresponding to the reverse voltage scan from 0.4 V to 0.3 V as the experimental data for regression fitting. The obtained decay of capacitor current over time, with *R-square =0.999*, is shown in equation 9. The exponential items with different time constants can be seen as three sub-capacitors, and the current-time curves of them were plotted in Figure 4(a). The complete charge and discharge times of the three sub-capacitances can be calculated by $5\times\tau$, i.e., 0.1810 s, 1.3455 s, and 4.6350 s, respectively. In equation 9, the value of c_2 is much larger than c_3, indicating that the long-tail current should be mainly contributed by the migration of iodine ions. It can be also observed from Figure 4(a) that the actual output current of a PSC is strongly determined by the step interval time Δt, which represents the duration after the voltage adjustment before the cell's current is measured. In the scanning of solar cell J-V curve, the value of step voltage ΔV (0.05 V here) is usually fixed. Therefore, Δt is inversely proportional to the scanning speed $\Delta V/\Delta t$. Consequently, hysteresis in the *J-V* curves of PSCs will strongly depend on the scanning speed, as illustrated in Figure 1(a).

$$I_c(t) = I_0(0.7898 * e^{-\frac{t}{0.0362}} + 0.1467 * e^{-\frac{t}{0.2691}} + 0.0637 * e^{-\frac{t}{0.9270}}) \quad (9)$$

According to equations 6 and 7 established in this paper, and the ionic capacitor model, the output current of PSC can be written as equation 10. This current model can be divided into two parts: the traditional equivalent circuit part, which can reflect the traditional steady photogenic current, and an extra capacitor part, which is proposed here to reflect the effect of the ion migration. For the carriers that respond rapidly to voltage changes and can quickly reach equilibrium after the application of a voltage change, we refer to the current output from the traditional equivalent circuit part, I_{trad}, as the steady-state current. In contrast, due to the slower response of ions to voltage changes, the current output from the extra capacitor part, I_c, is referred to as the non-steady-state photocurrent.

$$I = I_{trad} - I_c = I_{ph} - I_s\left(e^{\frac{q(U+I_{trad}R_S)}{nK_BT}} - 1\right) - \frac{U+I_{trad}R_S}{R_{sh}} - I_c \quad (10)$$

where I_{ph} is the photogenerated current, R_s is the series resistance, R_{sh} is the shunt resistance, the reverse saturation current can be written as $I_s = (I_{ph} - V_{oc}/R_{sh}) / exp(qV_{oc}/(nk_BT))$, and the ideal factor is fixed to be n =1.1.

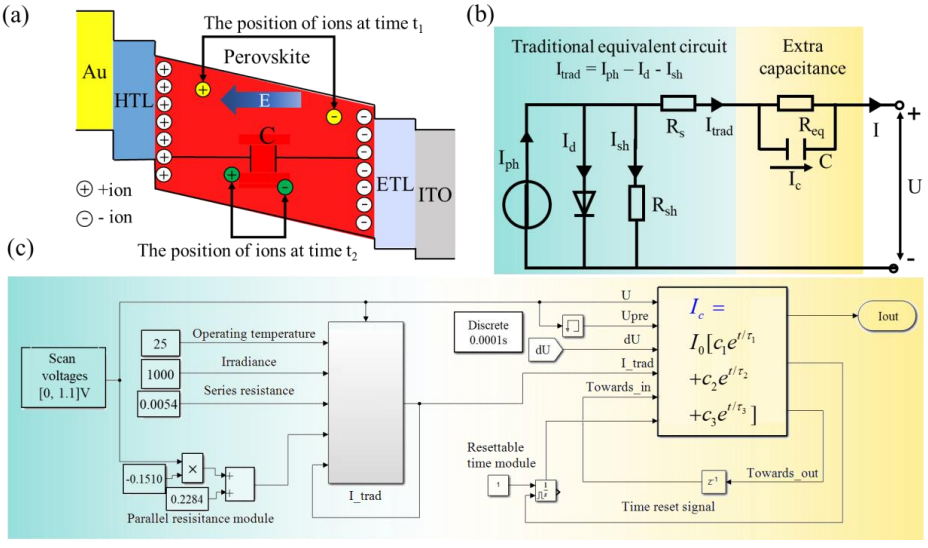

Figure 3 (a) Structure Diagram of PSC and the Positions of Ions at Different Time Points; (b) The Equivalent Circuit Model of a PSC with Hysteresis Effect; (c) PSC Matlab/Simulink Electrical Model

After the current model of PSC had been constructed, regression fittings were carried out to determine the parameters in

equation 10. The parameters that need to be determined are V_{oc}, I_{ph}, R_s, and R_{sh} , respectively. These parameters can be obtained by performing regression fitting on equation 10 using the stable *J-V* curve of a PSC, i.e., the current at a given voltage is measured after an adequate period. We derive the stable *J-V* curve of a PSC by averaging the currents in the forward and reverse scanning curves at every specific voltage, with a scanning speed of 200 mV/s, in Figure 1(a). Here, it should be noted that the *J-V* curve of PSC has a higher curvature than that of crystalline silicon cells. This is because, in PSCs, R_{sh} should be dependent on U as changes in operating voltage may cause extra leakage current related to ion migrations. Therefore, we tried to construct the relation between R_{sh} and U using a simple linear function $R_{sh}=gU+h$. After the regression fitting, the parameters obtained are $V_{oc}=1.0118$, $I_{ph}=20.0775$, $R_{sh}=-0.151U+0.2284$, and $R_s=0.0054$, respectively, with *R-square* =0.994.

Based on equations 10 and the structure of PSCs shown in Figure 3(a) we drew the equivalent circuit diagram of the PSCs, as shown in Figure 3(b), and we developed the electrical model of PSC in Matlab/Simulink, as shown in Figure 3(c), to simulate its *J-V* curves and long-tail current phenomena. The cyan-shaded area represents the I_{trad} component, while the yellow-shaded area represents the I_c component. For the I_{trad} component, we used a traditional crystalline silicon solar cell model to describe its dependence on scanning voltages. Then I_{trad} is used as an input parameter for the I_c component. I_c is calculated based on equations 6 and 7. At each scanning step, the scanning direction will be judged by comparing the values of the present input voltage U and the previous voltage U_{pre} (output a variable 'towards'); and if a voltage change has occurred ($U \neq U_{pre}$), a time reset signal will be generated which will cause the variable t in equation 6 to be reset to zero.

4 RESULT AND DISCUSSION

To verify the reliability and accuracy of the equivalent circuit model established in this work, at first, the hysteresis loop of the PSC *J-V* curve is simulated by Matlab/Simulink, using the same scanning speed as that of the experimental measurement. Corresponding results were shown in Figure 4(b), and for comparison, the measured results at scanning speeds of 200 mV/s and 1000 mV/s were given. It can be observed that the simulation results can perfectly reproduce the measured hysteresis loops at various scanning speeds. Then, the long-tail current in the hysteresis effect of PSCs was reproduced, as shown in Figure 4(c), which was obtained in reverse scanning with a stepwise voltage of 0.1 V and a duration of 5 seconds. The reproductions of both the hysteresis loops and long-tail currents together confirm the reliability and accuracy of the proposed equivalent circuit model with introduced exponential decay items.

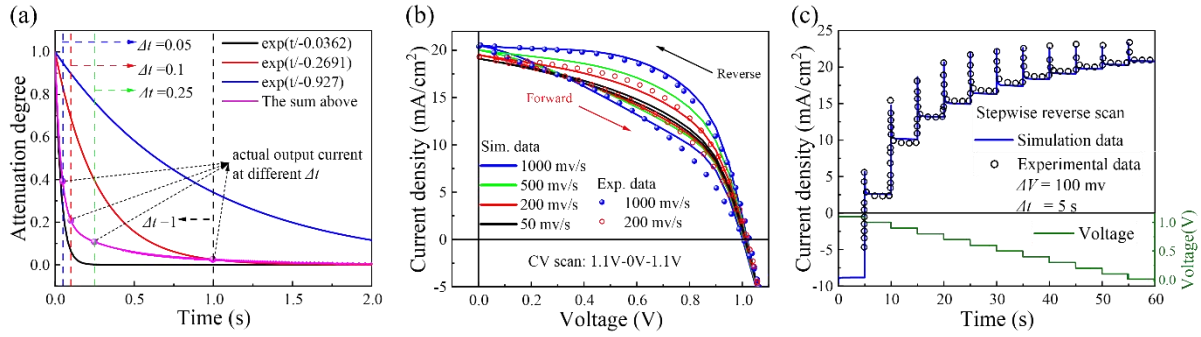

Figure 4 (a) Current Decay Curve of the Capacitor and Three Sub-Capacitances with Different Time Constants in PSC, $\tau_1=0.0362$, $\tau_2=0.2691$, $\tau_3=0.927$; (b) Hysteresis Loops of PSC at Different Scan Rates Simulated by Matlab/Simulink and the Experiment Data; (c) Simulation and Experiment Date of the Time-Dependent Photocurrent Response under Stepwise Reverse Scan with 100 mV Step Size and 5 s Step Time

By adjusting the parameters in the proposed model, some other typical hysteresis curves of different PSCs can also be reproduced[21]. For example, by adjusting I_0 at $U = 0$ *V* from 0 to 1.5, a special hysteresis curve was reproduced, where the reverse scan current consistently exceeded the forward scan current, as shown in Figure 5(a). According to the proposed model, such characteristic hysteresis curve should appear in high-quality PSCs with neglectable series resistance R_s. This is because, in these cases, when the voltage is adjusted from $U=0$ to ΔU (one scanning step), I_0 can be approximated as $I_0 \approx \Delta U/R_{load}$, where R_{load} can be evaluated by $\Delta U/J_{sc}$; therefore, I_0 should be greater than 0 when $U=0$ *V*.

In addition, in some cases the hysteresis curve may exhibit a phenomenon of current protrusion during reverse scanning, this phenomenon causes the short-circuit current to no longer be the maximum current that PSCs can generate. As shown in Figure 5(b), such a hysteresis curve can also be reproduced by increasing the values of I_0 around the protrusion position, specifically from 9 to 16. Such an adjustment is justifiable. In the case of a PSC possessing a moderate R_s, the values of $I_0 = U / (R_s + R_{eq})$ are expected to initially ascend and subsequently descend with the increment of voltage. This phenomenon can be evidenced by the measured results presented in Figure 1 (b).

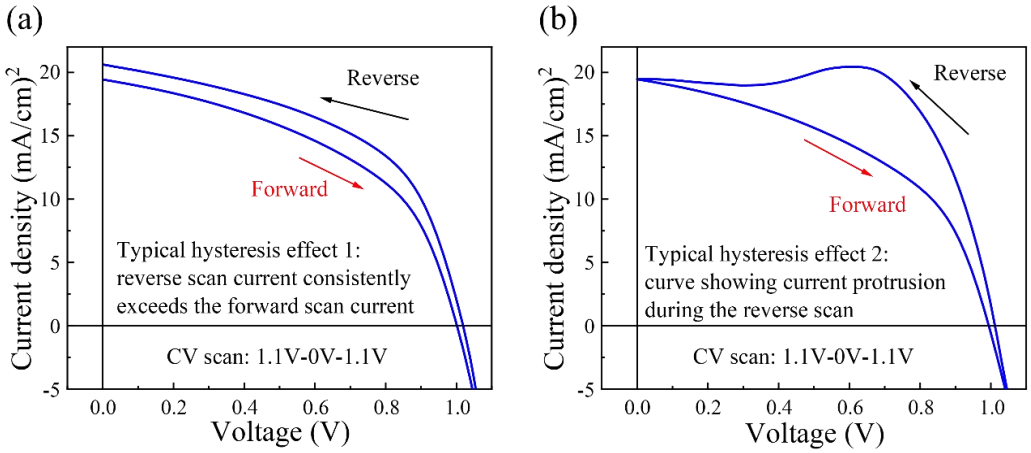

Figure 5 (a) Simulated Hysteresis Curve of a PSC Where the Reverse Scan Current Consistently Exceeds the Forward Scan Current; (b) Simulated Hysteresis Curve Showing Current Protrusion during the Reverse Scan

5 CONCLUSIONS

In conclusion, we propose an ionic capacitor model to describe the impact of ion migration on the current of PSCs. A voltage-related polynomial fitting approach was used to capture the complex relationship between the initial current and voltage; and the influence of ion migration on the current decay was represented as a linear combination of three sub-capacitors corresponding to electron, iodine ions, and other ions with lower mobilities. This model provides a more accurate representation of the ionic capacitor in PSCs. Building upon this framework, we propose an improved equivalent circuit model for PSCs by incorporating an additional ionic capacitance element into the conventional equivalent circuit. The model parameters can extract through regression fitting of available current *J-V* characteristics and current-time response curves. An electrical model of the PSC was then established on the Matlab/Simulink platform, and numerical simulations were performed using the proposed equivalent circuit model. The results demonstrate that the model not only accurately reproduces the hysteresis loop of PSCs, but also effectively captures their long-tail current characteristics; moreover, the model replicates and elucidates the hysteresis curves of two other typical PSCs, with key performance parameters exhibiting high consistency with experimental data. These insights are critically important for the optimization and development of PSCs based on MPPT algorithms.

COMPETING INTERESTS

The authors have no relevant financial or non-financial interests to disclose.

FUNDING

This work was supported by National Natural Science Foundation of China (Grant No. 52072121).

REFERENCES

[1] Wu S, Liu M, Jen AKY. Prospects and challenges for perovskite-organic tandem solar cells. Joule, 2023, 7(3): 484-502.
[2] Yang C, Hu W, Liu J, et al. Achievements, challenges, and future prospects for industrialization of perovskite solar cells. Light: Science & Applications, 2024, 13(1).
[3] Aydin E, Allen TG, De Bastiani M, et al. Pathways toward commercial perovskite/silicon tandem photovoltaics. Science, 2024, 383(6679).
[4] Du S, Huang H, Lan Z, et al. Inhibiting perovskite decomposition by a creeper-inspired strategy enables efficient and stable perovskite solar cells. Nature Communications, 2024, 15(1).
[5] National Renewable Energy Laboratory. 2025. https://www.nrel.gov/pv/cell-efficiency.html.
[6] Sarvi M, Azadian A. A comprehensive review and classified comparison of MPPT algorithms in PV systems. Energy Systems, 2022, 13(2): 281-320.
[7] Verma D, Nema S, Shandilya AM, et al. Maximum power point tracking (MPPT) techniques: Recapitulation in solar photovoltaic systems," Renewable and Sustainable Energy Reviews, 2016, 54: 1018-1034.
[8] B S, SKP D, S S, et al. Steady Output and Fast Tracking MPPT (SOFT-MPPT) for P&O and InC Algorithms," IEEE Trans. Sustain. Energy, 2021, 12(1): 293-302.

[9] Kang DH, Park NG. On the Current–Voltage Hysteresis in Perovskite Solar Cells: Dependence on Perovskite Composition and Methods to Remove Hysteresis. Advanced Materials, 2019, 31(34): 1805214 (2019).
[10] Kim H, Park N. Parameters Affecting I-V Hysteresis of CH3NH3PbI3 Perovskite Solar Cells: Effects of Perovskite Crystal Size and Mesoporous TiO2 Layer. The Journal of Physical Chemistry Letters, 2014, 5(17): 2927-2934.
[11] Tress W, Marinova N, Moehl T, et al. Understanding the rate-dependent J-V hysteresis, slow time component, and aging in CH3NH3PbI3 perovskite solar cells: the role of a compensated electric field. Energy & Environmental Science, 2015, 8(3): 995-1004.
[12] Anghel DV, Nemnes GA, Pintilie I, et al. Modelling J-V hysteresis in perovskite solar cells induced by voltage poling. Physica Scripta, 2019, 94 (12): 125809.
[13] Tang S, Yan J, Chen L, et al. Circuit modeling and analysis of hysteresis effect of perovskite photovoltaic cells. Solar Energy Materials and Solar Cells, 2024, 278: 113182.
[14] Seki K. Equivalent circuit representation of hysteresis in solar cells that considers interface charge accumulation: Potential cause of hysteresis in perovskite solar cells. Applied Physics Letters, 2016, 109(3): 33905.
[15] Gottesman R, Haltzi E, Gouda L, et al. Extremely Slow Photoconductivity Response of CH3NH3PbI3 Perovskites Suggesting Structural Changes under Working Conditions. The Journal of Physical Chemistry Letters, 2014, 5(15): 2662-2669.
[16] Hernández Balaguera E, Bisquert J. Time Transients with Inductive Loop Traces in Metal Halide Perovskites. Advanced Functional Materials, 2024, 34(6).
[17] Lopez-Varo P, Jiménez-Tejada JA, García-Rosell M, et al. Device Physics of Hybrid Perovskite Solar cells: Theory and Experiment. Advanced Energy Materials, 2018, 8(14): 1702772.
[18] Chen B, Yang M, Zheng X, et al. Impact of Capacitive Effect and Ion Migration on the Hysteretic Behavior of Perovskite Solar Cells. The Journal of Physical Chemistry Letters, 2015, 6(23): 4693-4700.
[19] Bisquert J. Hysteresis, Impedance, and Transients Effects in Halide Perovskite Solar Cells and Memory Devices Analysis by Neuron-Style Models. Advanced Energy Materials, 2024, 14(26).
[20] O'Kane SEJ, Richardson G, Pockett A, et al. Measurement and modelling of dark current decay transients in perovskite solar cells. Journal of Materials Chemistry C, 2017, 5(2): 452-462.
[21] Ravishankar S, Almora O, Echeverría Arrondo C, et al. Surface Polarization Model for the Dynamic Hysteresis of Perovskite Solar Cells. The Journal of Physical Chemistry Letters, 2017, 8(5): 915-921.